



ARL-TR-7576 • JAN 2016



Rail Shear and Short Beam Shear Properties of Various 3-Dimensional (3-D) Woven Composites

by Mark Pankow, Ashiq Quabili, Stephen Whittie, and Chian Yen

Approved for public release; distribution is unlimited.

NOTICES

Disclaimers

The findings in this report are not to be construed as an official Department of the Army position unless so designated by other authorized documents.

Citation of manufacturer's or trade names does not constitute an official endorsement or approval of the use thereof.

Destroy this report when it is no longer needed. Do not return it to the originator.



Rail Shear and Short Beam Shear Properties of Various 3-Dimensional (3-D) Woven Composites

by Mark Pankow
NC State University, Raleigh, NC

Ashiq Quabili
SURVICE Engineering Co., Belcamp, MD

Stephen Whittie
Oak Ridge Institute for Science and Education, Oak Ridge, TN

Chian Yen
Weapons and Materials Research Directorate, ARL

REPORT DOCUMENTATION PAGE

Form Approved
OMB No. 0704-0188

Public reporting burden for this collection of information is estimated to average 1 hour per response, including the time for reviewing instructions, searching existing data sources, gathering and maintaining the data needed, and completing and reviewing the collection information. Send comments regarding this burden estimate or any other aspect of this collection of information, including suggestions for reducing the burden, to Department of Defense, Washington Headquarters Services, Directorate for Information Operations and Reports (0704-0188), 1215 Jefferson Davis Highway, Suite 1204, Arlington, VA 22202-4302. Respondents should be aware that notwithstanding any other provision of law, no person shall be subject to any penalty for failing to comply with a collection of information if it does not display a currently valid OMB control number.

PLEASE DO NOT RETURN YOUR FORM TO THE ABOVE ADDRESS.

1. REPORT DATE (DD-MM-YYYY) January 2016		2. REPORT TYPE Final		3. DATES COVERED (From - To) December 2014	
4. TITLE AND SUBTITLE Rail Shear and Short Beam Shear Properties of Various 3-Dimensional Woven Composites				5a. CONTRACT NUMBER	
				5b. GRANT NUMBER	
				5c. PROGRAM ELEMENT NUMBER	
6. AUTHOR(S) Mark Pankow, Ashiq Quabili, Stephen Whittie, and Chian Yen				5d. PROJECT NUMBER	
				5e. TASK NUMBER	
				5f. WORK UNIT NUMBER	
7. PERFORMING ORGANIZATION NAME(S) AND ADDRESS(ES) US Army Research Laboratory ATTN: RDRL-WMM-B Aberdeen Proving Ground, MD 5069				8. PERFORMING ORGANIZATION REPORT NUMBER ARL-TR-7576	
9. SPONSORING/MONITORING AGENCY NAME(S) AND ADDRESS(ES)				10. SPONSOR/MONITOR'S ACRONYM(S)	
				11. SPONSOR/MONITOR'S REPORT NUMBER(S)	
12. DISTRIBUTION/AVAILABILITY STATEMENT Approved for public release; distribution is unlimited.					
13. SUPPLEMENTARY NOTES					
14. ABSTRACT The material responses of 6 different 3-dimensional (3-D) woven architectures have been evaluated via quasi-static mechanical testing. The 3-D woven architectures consist of S-glass fiber and SC-15 epoxy matrix. The 2 mechanical experiments, rail shear and short beam shear tests, have been conducted on the 3-D woven specimens to evaluate their linear elastic responses and obtain in-plane and through-thickness shear properties. Two main conclusions can be made from these studies: 1) The angle interlock architecture has the highest resistance to in-plane shear, and 2) in terms of through-thickness shear properties, orthogonal architectures have the smallest reduction; however, the layer-to-layer and angle interlock architectures provide a larger amount of energy absorption characterized by stable failure modes that are not typically seen in the orthogonal and laminated architectures.					
15. SUBJECT TERMS 3-D woven, through-thickness reinforcement, mechanical properties, short beam shear, rail shear, Z-fiber					
16. SECURITY CLASSIFICATION OF:			17. LIMITATION OF ABSTRACT	18. NUMBER OF PAGES	19a. NAME OF RESPONSIBLE PERSON
a. REPORT	b. ABSTRACT	c. THIS PAGE			Mark Pankow
Unclassified	Unclassified	Unclassified	UU	34	19b. TELEPHONE NUMBER (Include area code) 410-306-0732

Contents

List of Figures	v
List of Tables	v
Acknowledgments	vi
1. Introduction	1
2. Specimen Configurations	2
3. Materials	5
3.1 Fiber	5
3.2 Matrix	5
4. Fabrication and Void Content	5
4.1 Infusion	5
4.2 Void Content	6
5. Experiment	7
5.1 V-Notch Rail Shear	8
5.2 Short Beam Shear Test	9
6. Results and Discussion	10
6.1 V-Notched Rail Shear Results and Discussion	10
6.1.1 In-Plane Shear Modulus:	10
6.1.2 In-Plane Shear Strength:	10
6.2 V-Notched Rail Shear Specimen Failure Analysis	13
6.3 Short Beam Shear Test Results and Discussion	15
6.3.1 Shear Slope	15
6.3.2 Shear Strength	15
6.4 Short Beam Shear Test Specimen Failure Analysis	17
7. Conclusion and Discussion	20

8. References	22
List of Symbols, Abbreviations, and Acronyms	24
Distribution List	25

List of Figures

Fig. 1	Through-thickness reinforcement methods.....	1
Fig. 2	RUC model shown for each of the 3-D woven architectures	4
Fig. 3	Burnout scanned images of various 3-D woven composites	7
Fig. 4	Various in-plane material orientations for mechanical testing	8
Fig. 5	V-notched rail shear samples prepared and tested per ASTM D7078 ¹⁷ 8	
Fig. 6	Short beam shear test specimen with simplified test fixture shown in green.....	9
Fig. 7	Shear stress-shear strain curves from V-notched rail shear experiments	12
Fig. 8	V-notched rail shear specimen cracks on the surface with dye penetrant.....	14
Fig. 9	Load vs. deflection curves from short beam shear experiments.....	17
Fig. 10	Short beam shear specimens cracking in tension on the bottom of the specimen	18
Fig. 11	Short beam shear specimens cracking as viewed from the side	19

List of Tables

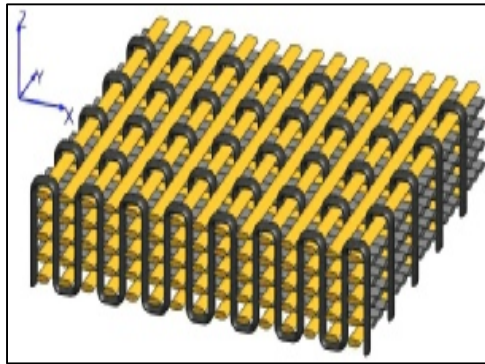
Table 1	Measured thicknesses and fiber volume fractions	3
Table 2	Fiber volume fractions	6
Table 3	Shear modulus (ksi)	10
Table 4	Shear yield strength (ksi)	10
Table 5	Shear slopes (lbf/in) obtained from short beam shear test.....	15
Table 6	Shear strength (ksi) obtained from short beam shear test.....	16

Acknowledgments

The authors wish to acknowledge Seth Ghiorse, Paul Moy, Tim Walter, Art Yiournas, and Jordan Wagner for their valuable feedback and assistance with experimental setups. The authors also wish to thank Textile Engineering and Manufacturing, Inc., for supplying the 3-dimensional woven preforms and Jim Wolbert for fabricating the panels.

1. Introduction

Traditional 2-dimensional (2-D) laminated composite materials are subject to delamination because they merely rely on matrix material to hold the individual layers together. To date, various methods of through-thickness reinforcement have been used to improve delamination resistance such as stitching, Z pinning, and 3-dimensional (3-D) weaving (Fig. 1). The stitching method uses needles to insert fiber strands through the thickness of the material and provides binding.^{1,2} The Z-pinning method inserts small pins via ultrasonic vibrating motions; however, each of these pins are independent and not connected to each other.³⁻⁵ Both of these methods tend to produce damages to the in-plane fibers from the insertion process.^{3,6} The 3-D weaving enables a way to integrally bind the individual layers together without initiating any damages into the preforms.⁷ Thus, 3-D woven composites provide a promising solution for mitigating the onset and spread of delamination failures in composite materials.⁸ Recent developments in Jacquard looms has enabled 3-D weaving technology to produce a variety of new architectures⁹ for reducing delamination. It is critical to understand the mechanical responses of these architectures to maximize their benefits.



3-D Weaving¹⁰ (Courtesy of Axis Composites Limited)
Fig. 1 Through-thickness reinforcement methods

Two different experimentations were conducted on 6 distinct 3-D woven architectures to determine the architectural effect on mechanical properties. The first experiment was a V-notched rail shear test to establish the in-plane shear modulus and shear strength of the architectures. A postfailure analysis was performed to determine any architecture-related features that could be identified. The second experiment was a short beam shear test to determine the effective through-thickness shear response of the material.

2. Specimen Configurations

The 6 different 3-D woven architectures described in this report were originally designed by the US Army Research Laboratory (ARL). The design specifications were provided to a textile weaver, Textile Engineering and Manufacturing (TEAM), Inc., for preform fabrications as a part of cooperative agreement between ARL and TEAM. The 3-D woven architecture properties were compared and evaluated with plain weave 2-D laminate composite samples (Base). An analysis of the yarn fraction in each orientation is shown in Table 1. The 3-D architecture configurations and the base configuration are briefly described as follows:

- The 3% Z-fiber: In this orthogonal 3-D design, approximately 3% of the total fiber was used as warp weavers (Z-fibers, orthogonal to the in-plane fibers). The Z-fibers wove all the way from the top surface to the bottom surface to interlock the in-plane fibers.
- The 6% Z-fiber: In this orthogonal 3-D design, approximately 6% of the total fiber used was warp weavers (Z-fibers, orthogonal to the in-plane fibers). The Z-fibers wove all the way from the top surface to the bottom surface to interlock in-plane fibers.
- The 10% Z-fiber: In this orthogonal 3-D design, approximately 10% of the total fiber used was warp weavers (Z-fibers, orthogonal to the in-plane fibers). The Z-fiber wove all the way from the top surface to the bottom surface to interlock the in-plane fibers.
- The 12° angle interlock: In this 3-D woven configuration, the warp weavers wove all the way from top surface to the bottom surface at $\pm 12^\circ$ angle to interlock the in-plane fibers.
- The 20° layer-to-layer: In this 3-D design, each warp weaver wove at $\pm 20^\circ$ to interlock 2 adjacent in-plane fiber layers.
- The 60° layer-to-layer: In this 3-D design, each warp weaver wove at $\pm 60^\circ$ to interlock 2 adjacent in-plane fiber layers.
- Base: This 2-D laminate was fabricated using 10 layers of 250 yield 24 oz/yd², 5 × 5 plain woven roving S-2 glass, with orthotropic layup [0]10.

Table 1 Measured thicknesses and fiber volume fractions

Configuration	Woven preform average thickness (inches)	Cured composite average thickness (inches)	Warp %	Weft %	Z-Fiber %
Base	...	0.25	50.0	50.0	...
3%	0.31	0.26	46.0	49.0	4.0
6%	0.36	0.26	45.0	48.0	7.0
10%	0.26	0.24	43.0	48.0	9.0
12°	0.32	0.24	49.0	51.0	...
20°	0.36	0.25	51.0	49.0	...
60°	0.35	0.25	50.0	50.0	...

For each of the 3-D woven architectures, the in-plane fibers were made using 250 yield S-2 glass, and the warp weavers were made of 1,250 yield S-2 glass fibers. Figure 2 illustrates the parametric representative unit cells (RUC) of the 3-D woven architectures as described. The warp weavers are shown as white in color, where the in-plane fibers are shown as red and or blue.

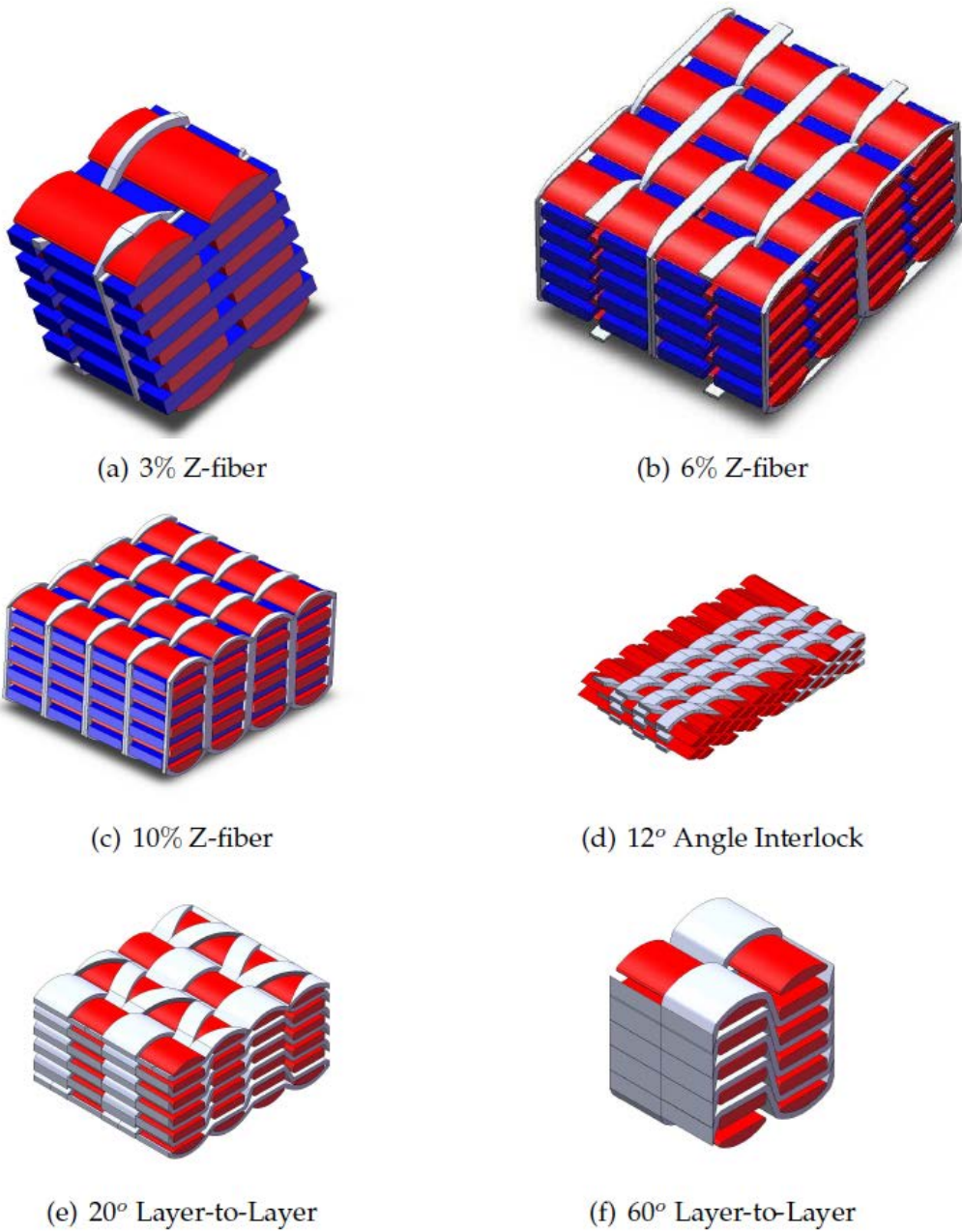


Fig. 2 RUC model shown for each of the 3-D woven architectures

3. Materials

3.1 Fiber

S-2 glass (AGY, Aiken, SC), used as the fibers in the weaving process, is a part of the magnesium-alumina-silicate-glass family of fibers. The individual properties under static loading are as follows¹¹:

- E_{11} : 114.2 GPa
- G_{12} : 46.5 GPa
- ν_{12} : 0.22

3.2 Matrix

SC-15 (Applied Poleramic, Inc., Benecia, CA), a thermosetting epoxy, was infused into the preforms. It is a low-viscosity 2-phased toughened epoxy resin system consisting of part A (resin mixture of diglycidylether epoxy toughener) and part B (hardener mixture of cycloaliphatic amine polyoxylalkylamine).¹² The mechanical properties of SC-15 are as follows:

- E_{11} : 2.487 GPa
- ν_{12} : 0.35
- σ_u : 110 MPa
- ϵ_u : 6.4%

4. Fabrication and Void Content

4.1 Infusion

Panels were made using a vacuum-assisted resin transfer molding system. See Pankow et al.¹³ for further details regarding panel fabrication.

4.2 Void Content

To determine the degree of impregnation, fiber burnout was performed to determine the void content of the specimens. This procedure is based on American Society for Testing and Materials (ASTM) standard D2734.¹⁴ The results of the burnout method are shown in in Table 2, which indicates the volume fractions and densities. According to the calculations, the void content is within the manufacture's specification. The postburnout images shown in Fig. 3 provide some details of the architectures and the movements of the Z-fiber in the different planes.

Table 2 Fiber volume fractions

Configuration	Fiber (%)	Matrix (%)	Voids (%)	Density (cm³)
Base	47.1	50.5	2.4	1.744
3%	45.2	51.8	3.0	1.713
6%	45.9	53.5	0.6	1.749
10%	45.2	52.0	2.8	1.715
12°	41.6	57.6	0.8	1.689
20°	40.3	58.8	0.9	1.671
60°	39.2	57.4	3.4	1.627

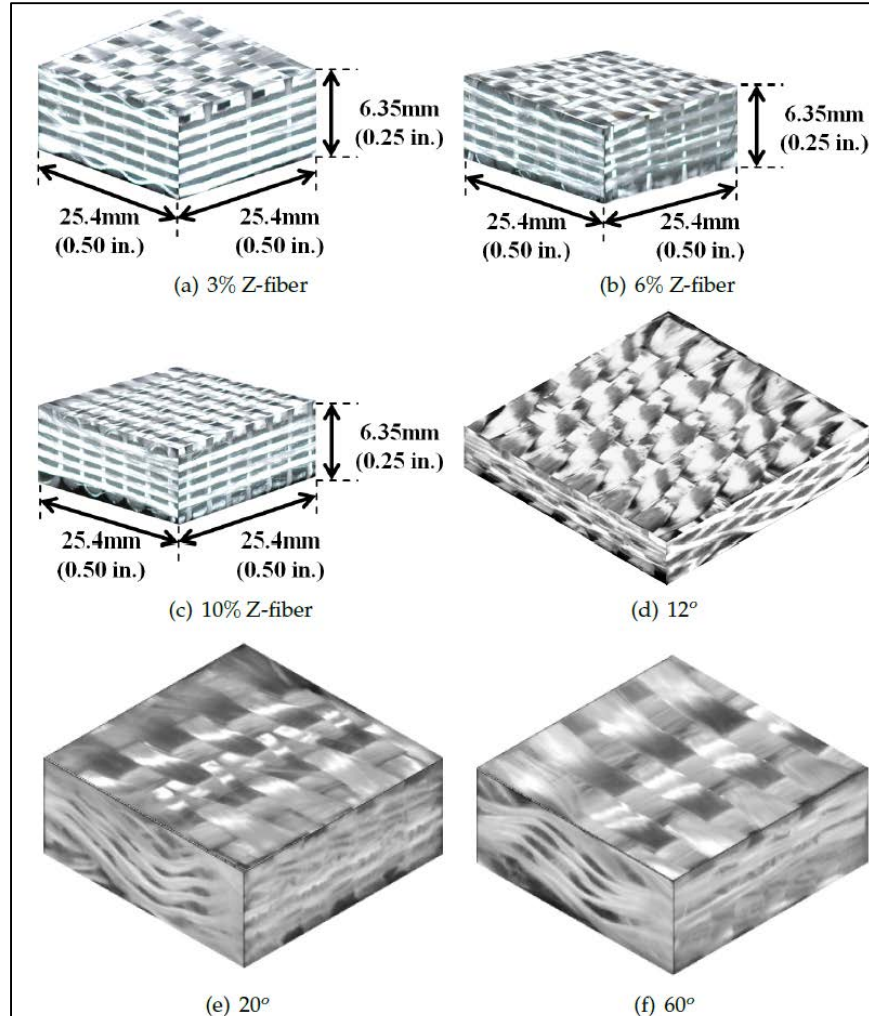


Fig. 3 Burnout scanned images of various 3-D woven composites

5. Experiment

The quasi-static rail shear and short beam shear tests were performed on the 6 different 3-D architectures as previously described. The data represents the average of 5 specimens that were repeatedly tested in the exact configuration. Testing was performed with 3 different orientations: 0° , 45° , and 90° . The orientations are as indicated in Fig. 4. These different orientations give insight to the weft (0°) and warp (90°) response and the 45° orientation. The results were compared with plain weave 2-D laminate properties.

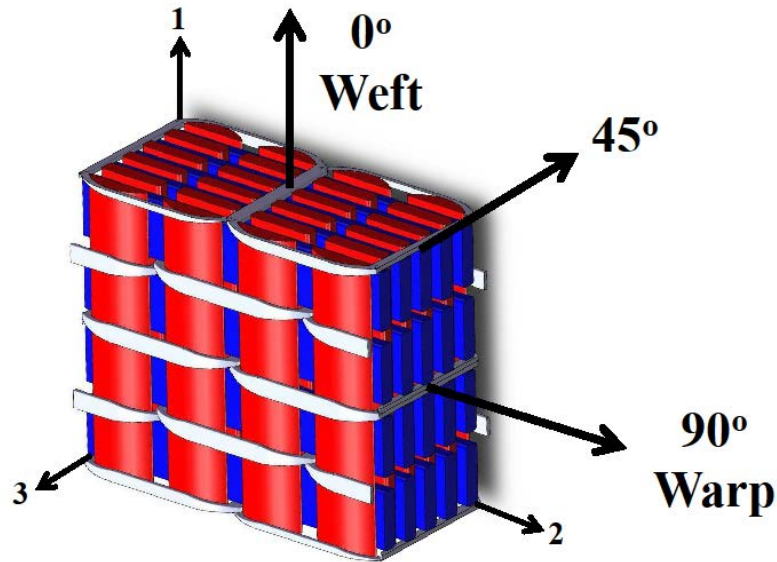


Fig. 4 Various in-plane material orientations for mechanical testing

5.1 V-Notch Rail Shear

V-notched rail shear tests were performed in accordance with ASTM standard D7078.¹⁵ Specimens were cut from quarter-inch-thick panels with overall dimensions of 3 × 2 inches with a shear notch length of 1.2 inches; a sample geometry can be seen in Fig. 5. Samples were loaded at a rate of 0.05 inch/min (1.0 mm/min). The stress was derived from the data from the load cell and specimen geometry, while the strain was derived from digital image correlation (DIC) measurements on the surface of the material. The DIC strain results were based on the average strain measured in the test section.

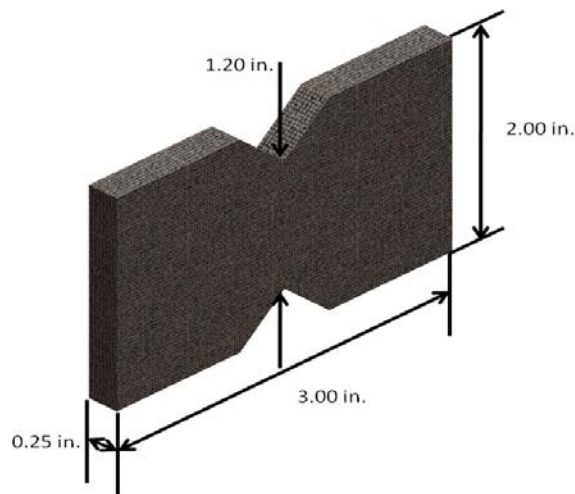


Fig. 5 V-notched rail shear samples prepared and tested per ASTM D7078¹⁵

5.2 Short Beam Shear Test

Short beam shear tests were performed in accordance with ASTM standard D2344.¹⁶ Specimens were cut from the quarter-inch-thick panels to produce relatively small specimens due to the fact that the width and length were twice and 6 times the thickness (0.25 inch) of the specimen, respectively (Fig. 6). The specimens were loaded at a rate of 0.05 inch/min (1.0 mm/min). The average and standard deviation values were obtained from 6 tested samples. The test results of the 3-D samples might not reflect the true properties of the material since the test standard was developed for laminated composites only. The effective inter-laminar shear strength can be calculated as follows:¹⁶

$$ILSS = \frac{3P_B}{4wt}, \quad (1)$$

where P_B is the maximum load, w is the width, and t is the thickness of the specimen.

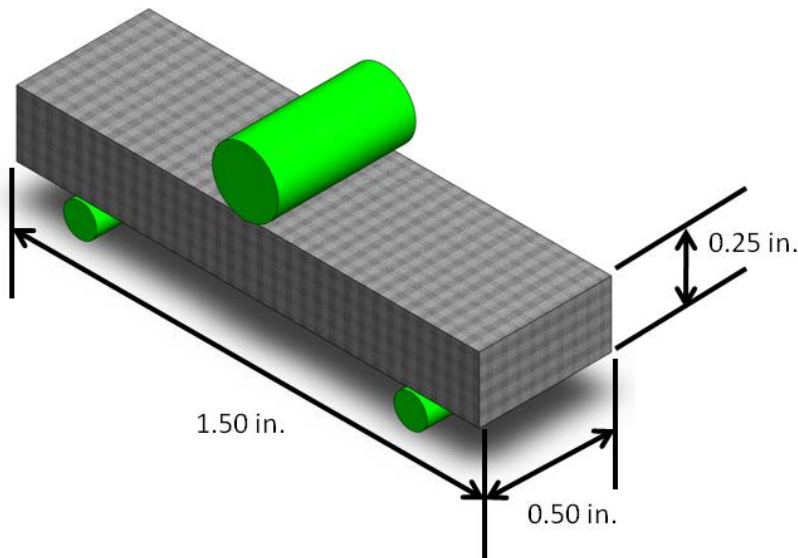


Fig. 6 Short beam shear test specimen with simplified test fixture shown in green

6. Results and Discussion

6.1 V-Notched Rail Shear Results and Discussion

6.1.1 In-Plane Shear Modulus:

Table 3 Shear modulus (ksi)

Configuration	0°	45°	90°
Base	840 ± 62	2,780 ± 194	840 ± 62
3%	830 ± 39	2,647 ± 30	790 ± 37
6%	746 ± 25	2,623 ± 69	767 ± 63
10%	794 ± 12	2,661 ± 24	807 ± 115
12°	1,018 ± 23	2,405 ± 94	972 ± 36
20°	802 ± 64	2,226 ± 58	766 ± 64
60°	808 ± 56	2,056 ± 168	863 ± 88

Typically, layer-to-layer configurations may indicate higher resistance to shear compared to orthogonal architectures because the inter-layer movements in layer-to-layer designs can provide additional reinforcements to shear. This assumption was not evident in the results shown in Table 3; however, it was observed that the 12° angle interlock architecture had the highest resistance to shear at 0° and 90° orientations. This was possibly related to the twisted nature of the 12° architecture, which formed a stronger binding of the tow bundles. The modulus obtained at the 45° orientation did not provide a meaningful comparison of the configurations because the load had not been directly transferred on the fiber bundles for this case. The results indicated that the Z-fiber architectures had some reduction in moduli. Among the orthogonal configurations, the 6% had the largest reduction in shear modulus—around 9% drop at both 0° and 90° orientations.

6.1.2 In-Plane Shear Strength:

The shear stress yield strength values obtained from the test are provided in Table 4.

Table 4 Shear yield strength (ksi)

Configuration	0°	45°	90°
Base	5.61 ± 0.16	23.61 ± 1.32	5.61 ± 0.16
3%	4.13 ± 0.13	20.73 ± 2.52	4.15 ± 0.15
6%	4.50 ± 0.10	16.45 ± 1.08	5.09 ± 0.32
10%	4.16 ± 0.28	18.82 ± 1.95	4.64 ± 0.32
12°	6.07 ± 0.08	25.04 ± 1.66	6.86 ± 0.11
20°	5.03 ± 0.34	20.49 ± 1.80	5.25 ± 0.10
60°	4.57 ± 0.17	17.19 ± 0.96	4.94 ± 0.12

The yield strength of the material was calculated from stress-strain response. A 0.2% plastic strain offset method was used to calculate the yield of the material. Table 4 compares the maximum shear strength for each of the architecture per orientation. At 45° orientation, yield stress could not be measured from the stress-strain curves as most of the samples did not have a yield. Therefore an ultimate strength was calculated instead. The results indicated that the 12° architecture produced the highest yield strength at each orientation. It was observed that all of the orthogonal Z-fiber configurations had a significant reduction (nearly 25%) in strength compared to the base. This might be due to an early onset of failure induced by the Z-fibers. Although the 6% had the highest reduction in shear modulus, it had the lowest reduction in shear strength compared to the other orthogonal configurations.

Shear stress-shear strain curves from the in-plane shear experiments are shown in Fig. 7. The curves indicated a bilinear response with a linear elastic portion and a plastic region where the progressive damages began to form in the samples. Based on the stress-strain curves, it was notable that the 12° configuration outperformed the other architectures in terms of shear strength and moduli. Another observation made from the curvatures was that the plastic portion of the base material showed a decrease in strength beyond its peak value. This was not the case for the 3-D woven architectures as the plastic zone of these materials indicated an upward slope. The 3-D materials had become more stable after initial failure likely caused by the matrix material and continued to carry further load through the fiber bundles. This indicated that under this type of loading condition, 3-D materials would likely exhibit higher energy absorption than 2-D materials.

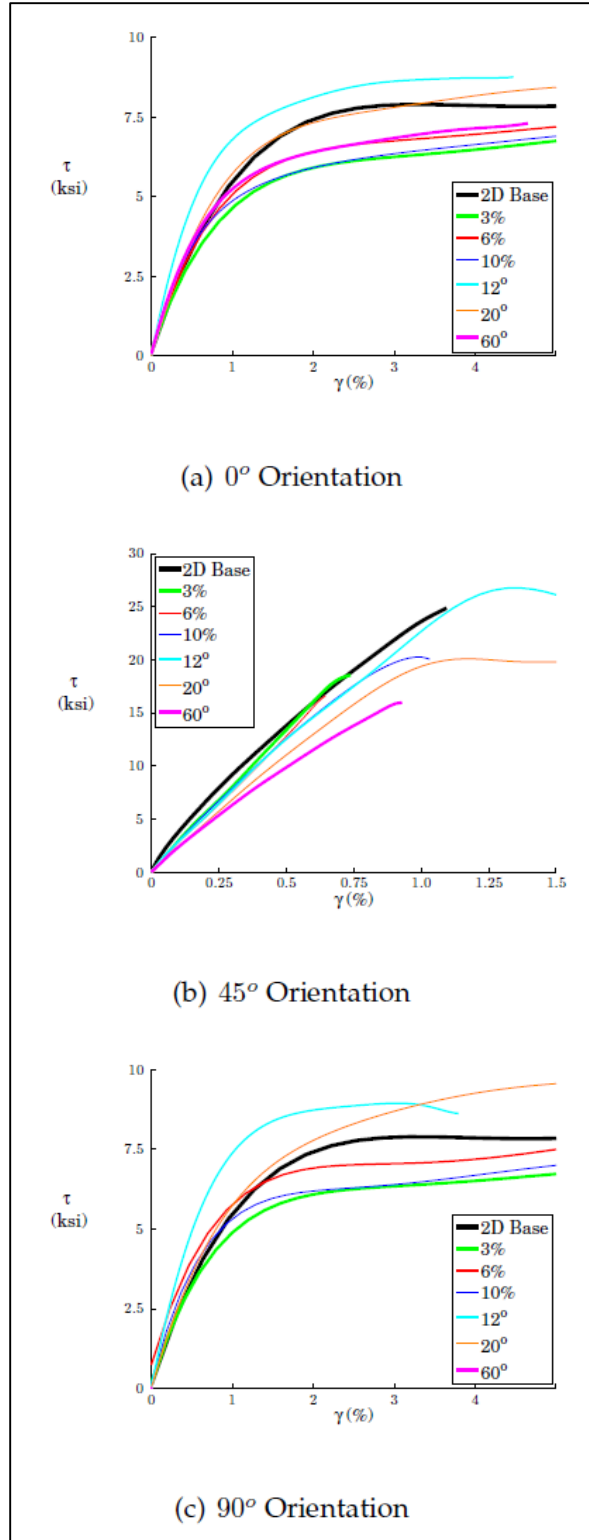


Fig. 7 Shear stress-shear strain curves from V-notched rail shear experiments

6.2 V-Notched Rail Shear Specimen Failure Analysis

The failed specimens were analyzed using a dye penetrant. Figure 8 shows images of the specimens after failure and dye penetration. Some of the surfaces of these samples showed architecture dependent cracking. For example, at 0° and 90° orientations, the orthogonal samples displayed surface crack formations that mimicked the Z-fiber patterns of the individual architectures. In the 6% samples, vertical cracks were visible that bridged 2 adjacent weft tows. In the 3% samples, cracks were formed along the Z-fibers, which bound a single weft tow. Additionally, it was noticed that most fiber yarns were no longer aligned with the original test orientations as they underwent plastic deformation to a degree.

It was difficult to analyze the failure modes of the layer-to-layer and angle interlock samples due to their complex architectures. For the 20° and 60° samples, a limited degree of cracks formed near the V-notch areas. It was assumed that the individual cracks were formed along the warp tows at 0° and 90° orientations. These specimens showed very little damages at the 45° orientation because the warp and the weft fibers had likely allowed the load to propagate to the core of the specimens.

For the 12° angle interlock samples, it appeared that the individual cracks were connected with each other, which was likely due to the load carried by the interlocking warp fibers after the initial failure. This observation could provide a possible explanation for the test results, which indicated that 12° samples absorbed a significant amount of energy.

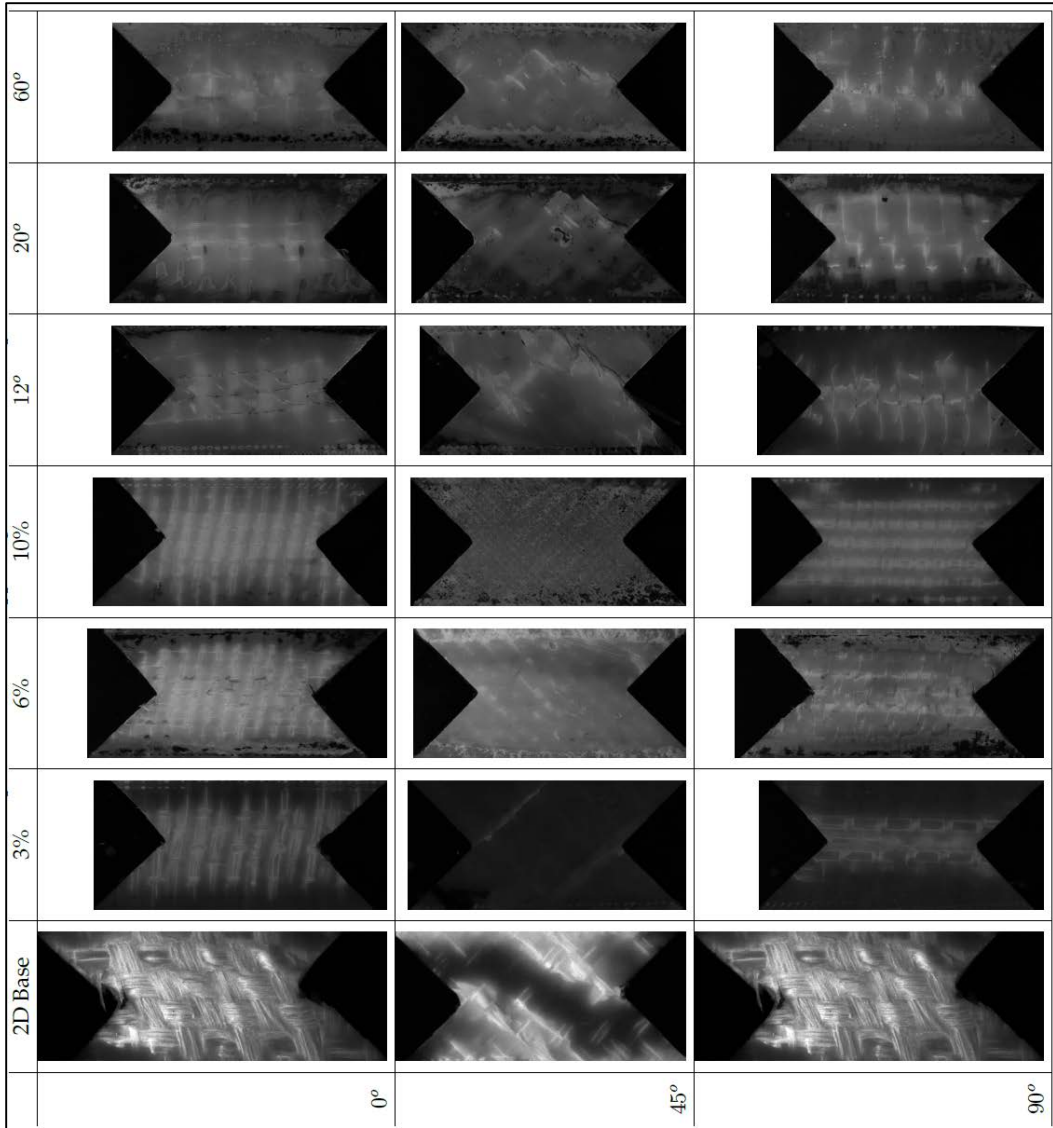


Fig. 8 V-notched rail shear specimen cracks on the surface with dye penetrant

6.3 Short Beam Shear Test Results and Discussion

6.3.1 Shear Slope

Table 5 provides a comparison of the effective stiffness of the materials. The effective stiffness was calculated by measuring the initial slopes from the load-displacement curves. Based on the results, at 0° orientation, the 6% Z orthogonal configuration had the highest effective bending stiffness. The base material and 3% Z-fiber configuration were second and third in ranking, respectively. The layer-to-layer architectures showed a considerable drop in bending stiffness. All of the 3-D materials demonstrated the highest stiffness response at 0° orientation. As previously mentioned, these materials had a lower property response at the 45° orientation because the individual fibers in the specimens did not directly carry the load. Comparing the data at 0° and 90° orientation, the 3-D materials had higher stiffness properties at 0° orientation because these configurations contained higher amount of weft (0°) fiber layers compared to the warp (90°) layers. In addition, the weft layers were always at a higher distance from the center of the specimen, which might have increased the bending stiffness.

Table 5 Shear slopes (lbf/in) obtained from short beam shear test

Configuration	0°	45°	90°
Base	21,855 ± 594	11,340 ± 435	21,855 ± 594
3%	21,369 ± 2331	11,147 ± 796	21,817 ± 250
6%	23,096 ± 665	8,949 ± 647	20,522 ± 913
10%	20,288 ± 1497	8,679 ± 166	17,305 ± 925
12°	17,166 ± 1609	11,198 ± 1825	17,985 ± 390
20°	16,941 ± 1261	9,152 ± 436	17,013 ± 553
60°	14,761 ± 3550	9,214 ± 850	16,323 ± 413

6.3.2 Shear Strength

Table 6 characterizes the shear strength of each of the architectures based on the maximum load in the material. The results indicated that the orthogonal configurations had relatively higher strength compared to the layer-to-layer and angle interlock 3-D configurations. Similar experimental results with additional details have been reported in Walter et al.^{17,18}

Table 6 Shear strength (ksi) obtained from short beam shear test

Configuration	0°	45°	90°
Base	5.42 ± 0.10	2.61 ± 0.04	5.42 ± 0.10
3%	5.38 ± 0.19	2.79 ± 0.04	4.99 ± 0.12
6%	5.31 ± 0.07	2.47 ± 0.02	4.87 ± 0.17
10%	5.49 ± 0.86	2.28 ± 0.03	4.27 ± 0.10
12°	4.75 ± 0.26	2.42 ± 0.07	3.29 ± 0.10
20°	4.46 ± 0.12	2.56 ± 0.11	3.63 ± 0.08
60°	3.76 ± 0.23	2.20 ± 0.11	2.85 ± 0.14

Fig. 9 showed the load-displacement curves obtained from the experiments. All of the curves had a linear elastic region followed by failure in the material. The layer-to-layer architectures indicated notable reduction in strength after the onset of failure compared to the other configurations. At 0° and 90° orientation, the 12° angle interlock and 60° layer-to-layer materials displayed upward slopes beyond their initial failure points, indicating an increase in strength. This could be advantageous in energy absorption since this behavior generally represents a stable energy dissipation mechanism.

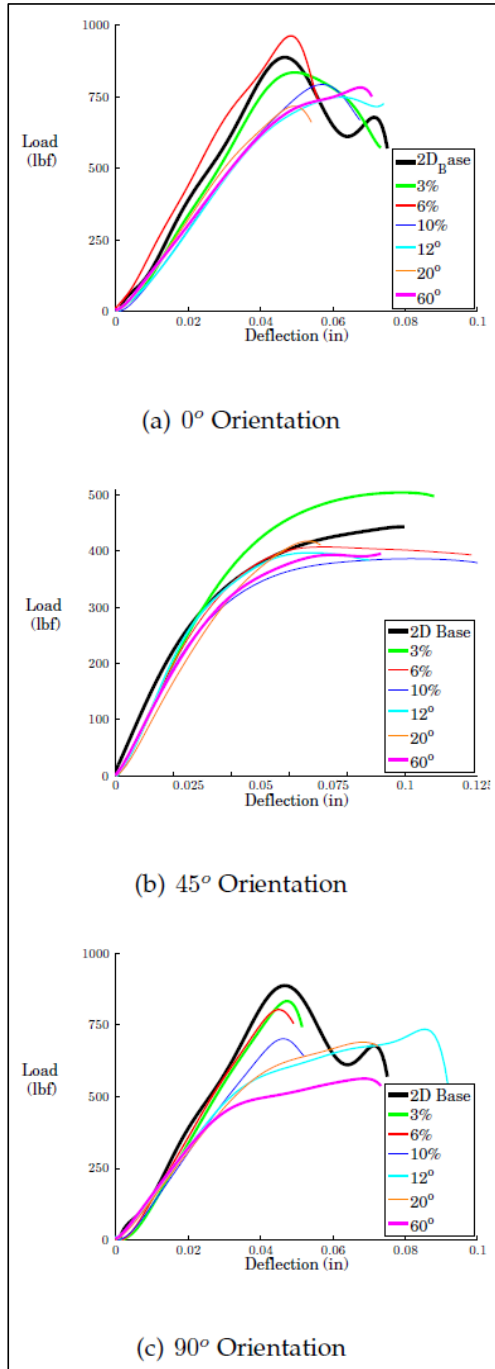


Fig. 9 Load vs. deflection curves from short beam shear experiments

6.4 Short Beam Shear Test Specimen Failure Analysis

To further understand the degree of damage induced in the specimens, a dye penetrant was placed on the surface of the specimen and illuminated under ultraviolet light. Figure 10 shows the tensile surface of the specimen. Figure 11 shows the side of the specimen where delamination was more visible. It was

difficult to evaluate the damages in the specimens as the extent of damages varied widely. This was because the specimens were run to different final displacements during the test. All of the architectures showed cracks forming along architecture dependent paths. These cracks formed at stress-concentrated areas, which were directly related to the architectural features. Similar failure modes in 3-D materials were noted by Walter et al.¹⁷

	0°	45°	90°
3%			
6%			
10%			
12°			
20°			
60°			

Fig. 10 Short beam shear specimens cracking in tension on the bottom of the specimen

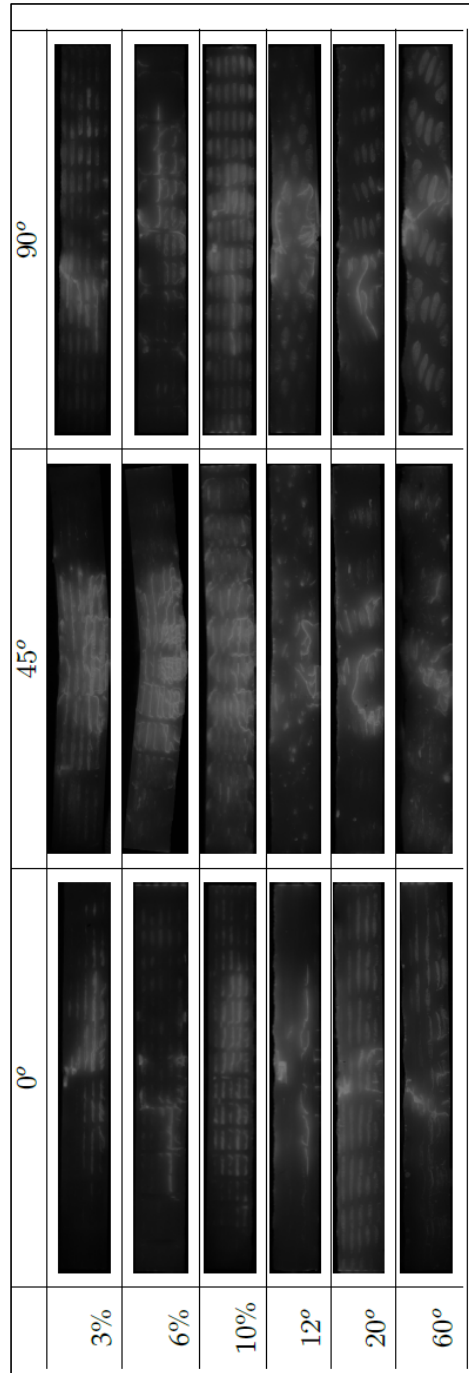


Fig. 11 Short beam shear specimens cracking as viewed from the side

While the 2-D base composite produced a widespread delamination, the 3-D architectures generated a limited amount of delamination. For the Z-fiber configurations, all of the specimens showed matrix crack formations due to tension. These cracks formed periodically. The space between 2 adjacent crack lines resembled the Z-fiber spacing of a representative architecture. Investigating the

sides of the specimens, it was visible that most of these cracks formed around the boundary of a fiber tow bundle and stopped progressing near the Z-fibers. Some of the cracks bridged across a matrix pocket where Z-fibers were not present. Additional cracks formed around the Z-fiber where the matrix material was loaded in tension.

The layer-to-layer and angle interlock 3-D configurations showed architecture dependent cracking as well. Because of the complexity of the architecture, it was difficult to pinpoint the characteristics of the cracks on this surface. The sides of the specimens (Fig. 11) showed that the cracks typically followed the path of a fiber tow bundle and oscillated through the thickness of the material. Some localized cracking was observed along with kink formations under the loading head from the compressive stresses. Overall, the layer-to-layer and angle interlock materials appeared to have lesser degree of damage due to the localized cracking. This could provide an explanation for the stable failure in these architectures identified in the load-displacement curves.

7. Conclusion and Discussion

Quasi-static V-notch rail shear and short beam shear tests were conducted on 6 different 3-D woven architectures including orthogonal, layer-to-layer, and angle interlock configurations to understand their in-plane and through-thickness shear responses. The results were compared with 2-D base materials. Overall, the results obtained from the 2 tests demonstrated that if the through-thickness shear properties of a material were to increase, the in-plane shear properties would likely decrease.

The results generated from rail shear test indicated that the angle interlock architecture provided the best resistance to shear. This could be due to the inter-layer movement of the fiber providing higher resistance. The orthogonal architectures exhibited a significant reduction in shear strength and modulus. This was a contrast from the previous study where the same orthogonal architectures did not indicate a major reduction in properties under quasi-static tensile and compressive loading conditions.¹³

The through-thickness shear responses of the material achieved from the short beam shear testing indicated that the 3% and 6% Z-fiber architectures demonstrated consistent through-thickness shear properties with minimal reduction in strength and moduli. The layer-to-layer and angle interlock architectures had a reduction in bending stiffness compared to that of the orthogonal and base configurations. This could have resulted from the waviness nature of the warp fibers. The load-displacement curves indicated that although the layer-to-layer and angle interlock architectures had a premature failure, they continued to carry further load after

initial cracks. This suggests that the delaminations were localized in these materials, which allowed them to sustain higher loads and dissipate large amounts of energy.¹⁷

Different damage modes had been investigated by Walter et al.¹⁸ that suggested that the through-thickness failure might originate from the reinforcement architecture. Damage modes were also investigated by conducting End Notch Flexure tests to study the interlaminar fracture toughness where the results showed steady crack propagation in orthogonal architectures and localized delaminations in layer-to-layer architectures under the loading head.¹⁹

8. References

1. Kang TLS. Effect of stitching on the mechanical and impact properties of woven laminate composites. *Journal of Composite Materials*. 1994;28(16):1574–1587.
2. Sharma S, Sankar B. Effect of stitching on impact and interlaminar properties of graphite/epoxy laminates. *Journal of Thermoplastic Composite Materials*. 1997;10:241–253.
3. Huang H, Waas A. Compressive response of z-pinned woven glass fiber textile composite laminates. *Composites Science and Technology*. 2009;69:2331–2337.
4. Mouritz A. Compression properties of z-pinned sandwich composites. *Journal of Materials Science*. 2006;41:5771–5774.
5. Cartie D, Partridge I. Delamination resistant laminates by Z-fiber pinning. *Composites: Part A*. 2005;36:55–64.
6. Clay S, Pommer A. Z-pin stubble technology advanced research (zs-tar). Wright-Patterson Air Force Base (OH): Air Force Research Laboratory (US); 2008 Apr. Report No.: AFRL-RB-WP-TR-2008-3107.
7. Cox B, Dadkhah M. The macroscopic elasticity of 3D woven composites. *Journal of Composite Materials*. 1995;29:785–819.
8. Mouritz A, Bannister M, Falzon P, Leong K. Review of applications for advanced three-dimensional fibre textile composites. *Composites: Part A*. 1999;30:1445–1461.
9. Yushanov S, Bogdanovich A, Mohamed M. Manufacturing and property analysis of a novel class of 3-D woven composites. *Journal of Thermoplastic Composite Materials*. 1999;12(1): 70–82.
10. Axis Composites Limited. Digital image [accessed 2014 Oct 7]. <http://www.axis-composites.com/3d%20weaving.html>.
11. Herakovich C. *Mechanics of fibrous composites*. 2nd ed. New York (NY): McGraw-Hill; 1998.
12. Zhou Y, Pervin F, Biswas M, Rangari V, Jeelani S. Fabrication and characterization of montmorillonite clay-filled SC-15 epoxy. *Materials Letters*. 2006;60:869–873.

13. Pankow M, Quabili A, Whittie S, Yen C. Tensile and laterally confined compression properties of various 3-dimensional (3-D) woven composites. Aberdeen Proving Ground (MD): Army Research Laboratory (US); 2014 Nov. Report No.: ARL-TR-7134.
14. ASTM D2734-94. Standard test method for void content of reinforced plastics. West Conshohocken (PA): ASTM International; 2003.
15. ASTM D7078. Standard test method for shear properties of composite materials by v-notched rail shear method. West Conshohocken (PA): ASTM International; 2012.
16. ASTM D2344. Standard test method for short-beam strength of polymer matrix composite materials and their laminates. West Conshohocken (PA): ASTM International; 2013.
17. Walter T, Subhash G, Sankar B, Yen C. Monotonic and cyclic short beam shear response of 3D woven composites. *Composites Science and Technology*. 2010;70(15):2190–2197.
18. Walter T, Subhash G, Sankar B, Yen C. Damage modes in 3D glass fiber epoxy woven composites under high rates of impact loading. *Composites: Part B*. 2009;40:584–589.
19. Pankow M, Salvi A, Waas A, Yen C, Ghiorse S. Resistance to delamination of 3D woven textiles composites evaluated using End Notch Flexure (ENF) tests: experimental results. *Composites: Part A*. 2011;42(10):1463–1476.

List of Symbols, Abbreviations, and Acronyms

2-D	2-dimensional
3-D	3-dimensional
ARL	US Army Research Laboratory
ASTM	American Society for Testing and Materials
DIC	Digital Image Correlation
RUC	Representative Unit Cells
TEAM	Textile Engineering and Manufacturing

- 1 DEFENSE TECHNICAL
(PDF) INFORMATION CTR
DTIC OCA
- 2 DIRECTOR
(PDF) US ARMY RESEARCH LAB
RDRL CIO LL
IMAL HRA MAIL & RECORDS
MGMT
- 1 GOVT PRINTG OFC
(PDF) A MALHOTRA
- 2 DIR USARL
(PDF) RDRL WMM A
A QUABILI
RDRL WMM B
C YEN

INTENTIONALLY LEFT BLANK.